Intrinsic Chirality Origination in Carbon Nanotubes

Neal Pierce[1], Gugang Chen[1], Lakshmy P. Rajukumar[1,2], Nam Hawn Chou[1], Ai Leen Koh[3], Robert Sinclair[3], Shigeo Maruyama[4,5], Mauricio Terrones[2] and Avetik R. Harutyunyan[1*]

[1]Honda Research Institute USA Inc., Columbus, OH 43212, USA

[2]Department of Physics, The Pennsylvania State University, University Park, PA 16801, USA

[3]Department of Materials Science and Engineering, Stanford University, Stanford, CA 94305, USA

[4]Department of Mechanical Engineering, The University of Tokyo, Tokyo, 113-8656, Japan

[5]Energy NanoEngineering Lab., The National Institute of Advanced Industrial Science and Technology, Tsukuba, 305-8561, Japan

Abstract

Elucidating the origin of carbon nanotube chirality is key for realizing their untapped potential. Currently, prevalent theories suggest that catalyst structure originates chirality via an epitaxial relationship. Here we studied chirality abundances of carbon nanotubes grown on floating liquid Ga droplets, which excludes the influence of catalyst features, and compared them with abundances grown on solid Ru nanoparticles. Results of growth on liquid droplets bolsters the intrinsic preference of carbon nuclei towards certain chiralities. Specifically, the abundance of the (11,1)/χ=4.31^o tube can reach up to 95% relative to (9,4)/χ=17.48^o, although they have exactly the same diameter, (9.156Å). However, the comparative abundances for the pair, (19,3)/χ=7.2^o and (17,6)/χ=14.5^o, with bigger diameter, (16.405Å), fluctuate depending on synthesis temperature. The abundances of the same pairs of tubes grown on floating solid polyhedral Ru nanoparticles show completely different trends. Analysis of abundances in relation to nucleation probability, represented by a product of the Zeldovich factor and the deviation interval of a growing nuclei from equilibrium critical size, explain the findings. We suggest that the chirality in the nanotube in general is a result of interplay between intrinsic preference of carbon cluster and induction by catalyst structure. This finding can help to build the comprehensive theory of nanotube growth and offers a new prospect for chirality-preferential synthesis of carbon nanotubes by the exploitation of liquid catalyst droplets.

Keywords

Carbon nanotubes, chiral-selectivity, liquid catalyst, kinetics, Zeldovich factor

The tremendous potential of carbon nanotubes[1] is hindered by one key factor: nanotube properties are delicately reliant on their chirality[2], and yet there is no established technology for chiral selective production. The root of the challenge is deeply fundamental – understanding the origin of chirality[3]. More than two decades of studies have revealed the essential contributions of a catalyst[4], its diameter[5], morphology[6-8], and composition and structure[9-13] in chirality abundance of grown nanotubes. Consequently, nowadays chiral-selectivity origination by catalyst structure via an epitaxial relationship emerges as a dominant mechanism[14-16]. However, it is hard to rule out the role of carbon nuclei structure for chirality origination, a scenario that has been realized in[17] by exploiting the proper molecular precursor as an embryo for specific nanotube cap. Targeting this dilemma in our strategy, we decided to decouple the influence of catalyst properties on the abundance of grown tube chiralities by exploitation of an isotropic surface of a floating liquid metal droplet as a catalyst. In comparison under the same synthesis conditions, we also exploit solid nanoparticles as a catalyst for revealing the impact of catalyst structure.

Results and Discussions

Gallium (Ga) and ruthenium (Ru) have been chosen as catalysts to ensure either liquid (melting point of Ga T_{bulk}=41^{o}C) or solid (melting point of Ru T_{bulk} =2441^{o}C) states for the complete range of temperatures (900^{o}C-950^{o}C) used for the synthesis of single walled carbon nanotubes (SWNTs). Growth of SWNTs via a catalytic chemical vapor deposition (CCVD) method on supported liquid Ga droplets[18] or on liquefied Fe catalysts[19,20] had been reported earlier. In this study, SWNTs were grown via a floating catalyst CVD method[21] but using Ga(acac) or Ru(acac) and ethanol as the catalyst and carbon sources, respectively (Fig. 1 and Materials and Methods). The growth produced tangled nanotubes with typical Raman radial breathing modes and G-bands. For both catalysts, the yields of grown nanotubes were relatively higher at 925^{o}C. Raman

characterizations were done with multiple laser excitation wavelengths including 488 nm, 532 nm, 632.8 nm, 830 nm and 1064 nm (Materials and Methods). On one hand, Raman RBM intensity had been shown by various groups to be strongly chirality dependent[22-24] and other variables such as the amount of defects could also affect the Raman cross-section[25-26]. On the other hand, SEM images shows that our samples had very low tube density while most tubes were short (~ 1-2um) in length. With a laser spot size of 1um and a spot-to-spot scanning step size of 10um, the possibility to count one tube multiple times or for multiple tubes with the same chirality located in one laser spot should be small. Based on these considerations, each RMB peak and its associated chirality was assigned to one individual carbon nanotube regardless of Raman intensity in the current work. Fig. 2a-c show the abundance of nanotubes depending on diameter grown on liquid Ga catalyst at different temperatures (Supplementary Information Table S2-S4). Insets in Fig.2a-c show that with an increase of temperature, the slight preference of smaller chiral angles ($\chi < 10^o$) transfers into a slight preference of larger chiral angles ($\chi > 15^o$), while the chiral angles in the range of $\chi = 10\text{-}15^o$ have consistent relatively high abundances (>20%) for all three temperatures. However, we noticed that the tubes with nominal diameters of 12.0Å ($\Delta d = \pm 0.2$Å, shadowed area), but with various chiralities corresponding to (14,2), (13,4), (15,0), (9,8), and (11,6), have significantly different abundances (up to fivefold), which change depending on temperature. Similarly, the tubes with relatively larger nominal diameter of 16.4Å ($\Delta d = \pm 0.2$Å, shadowed area) such as (20,1), (17,6), (19,3) and (18,5) also have significant differences in abundance. Taking into account that the tubes were grown on an isotropic surface of a liquid catalyst, this fact was very intriguing. To further study this trend, we decided to exclude nanotube diameter as a variable. For this aim, we carefully analyzed the temperature dependence of the abundances for two pairs of nanotubes. The first pair, (11,1) and (9,4), have

exactly the same diameter (9.156Å), but different chiral angles χ=4.31^o and χ=17.48^o, respectively. Similarly, the second pair, (17,6)/χ=14.5^o and (19,3)/χ=7.2^o, have exactly the same but relatively larger diameter (16.405 Å) in comparison with the first pair. These analyses open a unique opportunity to study nanotube chirality formation without the influences of catalyst structure, morphology, and diameter. For obtaining abundances of the above mentioned pairs by Raman spectroscopy, we used laser wavelengths λ=1064nm and 632nm for the (11,1)/(9,4) pair and 632nm and 532 nm for the (19,3)/(17,6) pair, respectively (Fig. 3), which provides close to the resonance excitations energies. Fig. 4a,b shows that for the pair of tubes (9,4) and (11,1), the smaller chiral angle χ=4.31^o corresponding to (11,1) chirality has apparent preference, especially at 950^{o}C where the preference reaches up to six fold. However, for the larger diameter pair of tubes (17,6) and (19,3) at 900^{o}C and 925^{o}C, the chiral abundance has almost the same value, but at 950^{o}C the large chiral angle χ=14.5^o, corresponding to (17,6) chirality is preferable. Hence, even when key catalyst parameters that are believed to determine tube chirality have been excluded, there is still a remarkable bias towards certain chiral angles such as χ=4.31^o or χ=14.5^o for a specific tube diameter. These results indicate that the carbon structure itself can originate chirality preference due to its own intrinsic mechanism of formation. In order to reveal the contribution of catalyst properties in the formation of nanotube chirality, we carried out analogical and comparative analysis of the abundances of tube chiralities grown on solid Ru nanoparticles Fig. 2 d-f (Supplementary Information Tables S5-S7) including (11,1)/(9,4) and (17,6)/(19,3) pairs. First, to validate the state of the Ru nanocatalyst during nanotube growth, we performed in situ environmental transmission electron microscopy (ETEM) studies of Ru nanoparticles at elevated temperatures (Fig.5). Structural analyses confirm that the particles are in the solid state and have various polyhedral forms. We didn't observe distinguishable structural

or morphological differences between 900°C and 950°C. Structural analyses among randomly chosen particles revealed that most of particles have energetically stable HCP structures, while some particles were either metastable FCC or had unknown structures. Twinning, which is common for cubic structures, was observed too. Similar to the tubes grown on Ga catalyst, the abundances of the chiral angles in the range of χ=10 -15^{o} are not only consistently high (Insets in Fig. 2d-f), but at 925^{o}C exceed 50%. Remarkably, the abundance of (11,3) tubes reaches almost 30%. However, in contrast to the growth on Ga catalysts, at 900^{o}C the smaller chiral angle nanotube (11,1)/χ=4.31^{o} is preferable, while the abundance of larger chiral angle became about two order higher with the increase of synthesis temperature (Fig 4 c, d). For the larger diameter nanotube pair of (17,6)/χ=14.5^{o} and (19,3)/χ=7.2^{o}, the abundance of the tubes with smaller chiral angle was preferential for all growth temperatures. Theoretical Kataura plots for the chirality assignments and corresponding typical representative Raman spectra for (11,1)/(9,4) and (17,6)/(19,3) pairs grown on solid Ru catalysts are shown in Fig. 6. Unlike liquid Ga, the solid Ru catalysts display various crystallographic structures and polyhedral shapes (Fig.5) with various exposed facets and presumably with various carbon-catalyst interfacial interactions. Therefore, the differences in the trends of chiral abundance of tubes grown on Ru catalysts when compared to Ga could be attributed to the influence of these properties. Hence, carbon structure intrinsically can bias towards specific chiral angles, while the influence of solid catalyst features can adjust it.

Observation of significant differences in abundance (up to 35 times based on spectral intensities) for tubes with exactly the same diameter (6,5) and (9,1) grown on solid catalysts Co/Mo and Fe/Co by CVD method have been associated to the stability of the carbon cap edge[27] and structures[28], respectively. Similarly, disproportion in the abundances of (6,6) and (7,5) with same

nominal diameters grown at various temperatures on solid Co catalysts have been associated with the constraints for cap formation energies[14,29]. Recently, it was reported that while there is no significant difference between the energies of carbon caps that could create bias towards specific chiral angles, the nanotube-catalyst interface might introduce chiral angle bias[30]. These arguments could be applied to our results for understanding the chirality bias in abundances of (11,1)/(9,4) and (17,6)/(19,3) pairs grown on Ru catalysts (Fig. 3c,d). Yet, the liquid state of the catalyst flattens the carbon–catalyst contact energy landscape by making the carbon-catalyst contact energies effectively equal[31]. As a result, the abundance of a given tube becomes nearly proportional to chiral angle[32,33]. On the contrary, in our experiments, the abundances of the pair of tubes (11,1)/(9,4) are biased towards smaller angle (11,1)/χ=4.31^{o}. This fact suggests that the observed differences in abundance cannot be the result of growth rate differences for various chiralities. Moreover, for the pair of tubes with bigger diameter, (17,6)/(19,3), grown on Ga droplets, the relative abundances fluctuate depending on growth temperature, and cannot be explained based on known models. Hence, all currently established variables that could create chiral angle bias, such as the properties of catalyst, energy preferences of carbon caps, carbon-catalyst interface energy and nanotube growth rates have been eliminated.

We analyze our experimental results in the frame of kinetic theory of nucleation, i.e., considering nucleation as a random process and thereby obeying to statistical laws. Current experimental and theoretical studies suggest carbon caps (comprises 6 pentagons) as seed for formation of nanotube chirality[17,34,35]. According to the census of carbon caps[36] there are 99 possible carbon caps with various isolated pentagon configurations that can initiate growth of (11,1) tubes and 99 caps for (9,4) tubes. For nanotubes with chiralities (19,3) and (17,6) this number is even bigger: 104,371. Furthermore, the number of carbon atoms in the caps of (11,1) and (9,4) tubes

generated by the Chemical and Abstract Graph Environment CaGe[37] vary from 48 to 86 for (11,1) caps and from 45 to 75 for (9,4) caps. For chiralities (19,3) and (17,6) the numbers of carbon atoms with isolated 6 pentagons are in the range of 96-354 and 93-311, respectively. To compute the energetics of all of these clusters would be beyond the available computation power. However, since number of nuclei grown in given interval of time is a random quantity due to the attachment and detachment processes then instead we can consider the probabilities P(n) of grown nucleus in order to compare with observed abundances in our experiments. Within the kinetic theory of nucleation this probability for heterogeneous nucleation of 2D clusters is defined as[38]

$$P(n) = \frac{1}{2}\left\{1 + erf\left[Z\sqrt{\pi} \times (n - n^*)\right]\right\} \quad (1)$$

where erf(x) is the error function and Z- is the Zeldovich factor[39,40]

$$Z = \frac{1}{\Delta n} = \frac{1}{2n^*} \times \sqrt{\frac{\Delta G^*}{\pi k_B T}} \quad (2)$$

where $\Delta G^*/k_BT > 3$. Z defines the width of deviation interval ΔG(n) of Gibbs free energy profile in the vicinity of critical size n* of carbon cluster defined as $\Delta n = n_{max} - n_{min}$, where the difference between nuclei free energy and formation barrier ΔG*(n=n*) is less than thermal energy k_BT (Fig.7). In other words, the overall nucleation rate is determined by the nucleation kinetics in the interval of Δn near critical nuclei size n*. This means that the "flatter" free energy profile ΔG(n) corresponds to the larger number of nucleus in k_BT range that can reach or overcome the critical size and continue growing. The inequality $\Delta G^*/k_BT > 3$, in practice is always valid for our experimental conditions, since in our synthesis kT ~ 0.1eV and ΔG ≥ 1eV[33,34]. Hence, by definition P(n)=0 when $n < n^* - \Delta n/2$ and P(n) = 1 when $n > n^* + \Delta n/2$. So,

we consider P(n) as the probability that a given carbon cluster will grow and reach a size that contains six pentagons.

From Fig. 4a,b, we converted the ratio of abundances of tubes grown on Ga droplets at 950^{o}C into probabilities. Solving the equation (1) relative to n (taking into account that erf(x) ~ x if -0.62 ≤ x ≤ 0.62) one obtains $n = n^* + 0.32\Delta n$ for the size of clusters of a (11,1) tube and $n = n^* - 0.32\Delta n$ for (9,4) chirality ($Z = 1/\Delta n$). Hence, carbon clusters that led to the tubes with (9,4) chirality dominantly are in the range of $n < n^*$, while for (11,1) the nucleus consist of number of carbon atoms $n > n^*$ (Fig. 7a). Accordingly, clusters that fit for nucleation of (9,4) tubes are subnuclei and tend to decay and thereby the abundance is very low. On the contrary the clusters for (11,1) tubes are supernuclei and tend to grow further and as a result have higher abundance. For chiralities (19,3) and (17,6) apparently, the $\Delta G(n)$ energy profile in the vicinity of equilibrium critical nuclei is "flatter" $\Delta n_{(19,3)/(17,6)} > \Delta n_{(9,4)/(11,1)}$ (Fig. 7b). This suggests that the nucleation barriers for the clusters that consist of carbon atoms $n_{min} < n^* < n_{max}$ are very close. Similarly to (9,4)/(11,1) pair, by using abundance data for this pair from Fig. 4b, we obtain nucleus sizes $n = n^* + 0.11\Delta n$ (supernuclei) and $n = n^* - 0.11\Delta n$ (subnuclei) for (19,3) and (17,6) tubes, correspondingly. Unlike the (9,4)/(11,1) pair, the nucleus sizes of the (19,3)/(17,6) pair are located in very close vicinity of the equilibrium critical size of nuclei n^* (Fig. 7b), which explains the observed fluctuations of relative abundances depending on growth temperature. Analogical calculations for abundances of (11,1) and (9,4) pair of nanotubes grown on Ru nanoparticles at T=925C resulted $n = n^* + 0.14\Delta n$ and $n = n^* - 0.14\Delta n$, respectively. For (11,1)/(9,4) pair grown at T= 950C as well as for (17,6)/(19,3) for all growth temperatures the condition erf(x) ~ x does not fulfilled due to high ratios of abundances, therefore it is impossible to obtain analytical solutions. From the above analysis (Fig. 7), it became apparent that for

successful growth of a carbon nuclei into a nanotube, it is not enough for nuclei to possess low nucleation energy, but it also needs to accommodate number of carbon atoms larger than equilibrium critical size n > n*. Once the nuclei size n > n*+0.5Δn the probability of decay is negligible.

Note that we assumed the same n^* and G^* in order to show both chirality pairs on one nucleation graph in Fig. 7 while in fact both parameters can be chirality dependent. Our assumptions could be partially justified considering: (1) Using the same critical size n^* does not change the relationship P(11,1) >P(9,4); (2) Theoretical calculations had demonstrated that the end cap edge energies for tubes with different chiralities but similar nominal diameters were almost the same[30]; (3) The Gibbs free energy of 2D nuclei was calculated to be equal to one-half of their edge energy[41].

Conclusion

For nanotubes grown on liquid catalyst droplets, nucleation kinetics can create chiral preference even for tubes with exactly the same diameter and similar nucleation energy barriers, despite a large variety of possible nuclei. The preference toward certain chirality can be predicted by knowing the critical nuclei size (n*), Zeldovich factor (Z), and the number of atoms in a given carbon nuclei (n). Consequently, controlling these parameters can lead to chirality preferable growth of the tubes. One way to achieve this is to create experimental conditions that provide a very narrow range of Δn (or larger Z) and range of $\Delta G(n^*) - \Delta G(n = n_{max}, n_{min}) \leq k_B T$ (shadowed areas in Fig.7). Apparently, growth of tubes with smaller diameters satisfies this requirement since the number of possible nuclei/caps are dramatically reduced (i.e. Δn is small). Yet, a more general approach that can lead to selective growth is variation in the degree of supersaturation.

Since the Zeldovich factor is $Z \sim (\Delta\mu)^2$ ($\Delta\mu$ – difference between chemical potentials of vapor and solid phases of carbon) then increasing $\Delta\mu$ will reduce Δn, which implies the possibility to achieve preferential/selective growth. This can be achieved by the bigger perturbation of the pressure P (or temperature) from its saturated equilibrium value (P_o) $\Delta\mu \sim \ln P/P_o$, which creates larger supersaturation (undercooling) and thereby becomes a driving force for the nucleation. In addition, if possible, synthesis at lower temperatures will also increase the selectivity by narrowing the range of $\Delta G(n^*) - \Delta G(n = n_{max}, n_{min}) \leq k_B T$. On the other hand, the presence of a catalyst with crystallographic structure, as is the case with nanotubes grown on Ru nanoparticles, reduces the formation energy of the grown carbon nuclei depending on their configurations and adhesion energies. Apparently, this reduction is more dramatic if there is an epitaxial relationship between these two structures. These changes in the energy also change the corresponding key parameters that define the nucleation probability: Zeldovich factor and critical nuclei size. As a result, the abundance of grown tubes chiralities becomes different in comparison with abundance statistics grown on liquid catalyst.

We expect that revealed dualism in nanotube chirality origination would help to create a comprehensive theory of nucleation and growth by considering the role of nucleation kinetics in chirality distribution. It can ignite a new strategy to achieve chiral selective/preferential growth based on liquid catalyst droplets, since unlike solid catalysts, in the case of a liquid catalyst, the number of variables are dramatically reduced. This method implies that thorough control of catalyst diameter is critical although this requirement is common among all reported methods aiming at chirality-controlled growth. We believe that the exploitation of colloidal Ga clusters with predetermined dimeter (smaller is preferable) and narrow diameter distribution could be an

effective approach. Our method in combination with low temperature and/or high pressure synthesis conditions may lead to selective/preferential growth.

Methods and Materials

Synthesis: Nanotubes were grown at ambient pressure via a floating catalyst CVD method using gallium (III) acetylacetonate $Ga(C_5H_7O_2)_3$/[$Ga(acac)_3$] and ruthenium (III) acetylacetonate $Ru(C_5H_7O_2)_3$/[$Ru(acac)_3$] and ethanol as the catalyst and carbon sources, respectively. Solutions (0.4 wt. %) of $Ga(acac)_3$ or $Ru(acac)_3$ dissolved in ethanol were prepared through mild sonication. The solution was then loaded into a syringe and delivered into a quartz tube furnace through a capillary connected to a syringe pump. The capillary was placed such that its exit point was just outside the hot zone of the tube furnace. The substrates (300 nm SiO_2 on Si) were loaded into the center of the quartz tube furnace, which was heated to the growth temperature (900^oC-950°C) under a constant flow of argon (450 sccm) and hydrogen (75 sccm). After the furnace reached the growth temperature, the Ga or $Ru(acac)_3$ / ethanol mixture was injected continuously into the tube furnace at a rate of 6 ml/hr for the duration of the nanotube growth (5 min – 15 min). At the end of the growth period the furnace was turned off and allowed to cool down to room temperature under the Ar/H_2 flow. For each temperature we synthesized three samples based on each catalyst in order accumulate more statistical data and reveal consistent pattern.

Raman mapping analysis of as-grown SWCNTs: Raman measurements were performed by a Renishaw inVia confocal micro-Raman spectrometer equipped with CCD detectors. Multiple laser lines including 488, 532 nm, 632.8 nm, 830 nm and 1064 nm were used to excite the samples. At least 2 or 3 separate samples at each temperature were used for the analysis. The sample was placed on an *x*-*y* piezo-stage and raster scanned with a step size of 10 μm for both *x* and *y* directions. A typical Raman mapping area consists of 121 individual scanning spots, while a minimum of 3 selected mapping areas were done on each sample. Usually more mapping areas were done for more RBM-dilute samples. So, the total number of spots scanned for each growth temperature can easily exceed 1000. The laser spot was ~1 μm with a 50 x long objective. The laser power at each wavelength was always kept at minimum in order to avoid heating. All Raman measurements were performed at room temperature. For chirality assignment, the following criteria were applied: transition energy $\Delta E = \pm 0.1$eV, Raman frequency window for radial breathing modes (RBM) $\Delta\omega = \pm 4$ cm^{-1} and signal/noise ratio S/N ≥ 3. Abundances of nanotubes have been obtained based on the total counts of corresponding RBMs $\omega_{RBM}=12.5+223.5/d$, where ω_{RBM} is the radial breathing mode (RBM) frequency and d is the tube diameter, was used in the Kataura Plot. For equal diameter pairs of tubes, we studied three samples for each growth temperature of 900^oC, 925^oC and 950^oC by using 532nm, 632.8nm and 1064nm excitations and scanning 1089, 1089 and 1331 spots for each sample, respectively. In these cases, for chirality assignment a Raman frequency window $\Delta\omega = \pm 1$ cm^{-1} was applied. As presented in Fig.2, the histograms show the sum of the statistics of all three samples. As an example, we also show in Fig. S1 of Supplementary Information the chirality distributions of nanotubes grown on Ga catalyst at 925°C from three different runs under identical growth conditions.

Environmental Transmission electron microscopy (ETEM): The experiments are performed on an FEI 80-300 environmental Titan TEM operated at 300 kV in high vacuum mode. The microscope is equipped with a spherical aberration (image) corrector for the TEM objective lens. Heating experiments were carried out using a DensSolutions Wildfire double-tilt MEMS-based heating holder. The Ru nanoparticles are suspended in ethanol, and dropcast on the compatible XT nanochip which is coated with a 20 nm thick SiN membrane.

Scanning electron microscopy (SEM): Post-growth micrographs of the samples were obtained on a Zeiss Ultra 55 FE-SEM with a 3mm working distance and accelerating voltage of 1 kV.

References

1. De Volder, M.F.L., Tawfick, S.H., Baughman, R. H. &Hart, A.J. Carbon nanotubes: present and future commercial applications. *Science* **339,** 535-539 (2013)
2. Saito, R., Dresselhaus, G., Drsselhaus, M.S. *Physical Properties of Carbon nanotubes*. Imperial College Press: London, 1998
3. Iijima, S. & Ichihashi, T. Single-shell carbon nanotubes of 1-nm diameter. *Nature* **363,** 603-605 (1993)
4. Harutyunyan, A.R. The Catalyst for growing single-walled carbon nanotubes by catalytic chemical vapor deposition method. *J. Nanosci. Nanotechnol*. **9**, 2480-2495 (2009)
5. Zhang, F. et al. Growth of semiconducting single-wall carbon nanotubes with narrow band-gap distribution. *Nature Commun*. **7,** 11160 (2016)
6. Zhu, H. et al. Atomic-Resolution imaging of the nucleation points of single-walled carbon nanotubes. *Small* **1**, 1180-1183 (2005)
7. Moors, M. et al. Early stages in the nucleation process of carbon nanotubes. *ACS Nano* **3**, 511-516 (2009)
8. Harutyunyan, A.R. et al. Preferential growth of single walked carbon nanotubes with metallic conductivity. *Science* **326**, 116-120 (2009)
9. Chiang, W.H. & Sankaran, R.M. Linking catalyst composition to chirality distributions of as-grown single walled carbon nanotubes by tuning Ni_xFe_{1-x} nanoparticles. *Nature Mater*. **8**, 882-886 (2009)
10. Yang, F. et al. Chirality-specific growth of single walled carbon nanotubes on solid alloy catalysts. *Nature* **510**, 522-524 (2014)
11. Wang, H. et al. Chiral-selective CoSO4/SiO2 catalyst for (9,8) single-walled carbon nanotube growth. *ACS Nano* **7**, 614-626 (2013)
12. Homma, Y., Liu, H., Takagi, D. & Kobayashi, Y. Single-walled carbon nanotube growth with non-iron-group "catalysts" by chemical vapor deposition. *Nano Res*. **2**, 793-779 (2009)
13. He, M. et al. Selective growth of SWNTs on partially reduced monometallic cobalt catalyst. *Chem. Commun*. **47**, 1219-1221 (2011)
14. Reich, S., Li,L. & Robertson, J. Control the chirality of carbon nanotubes by epitaxial growth. *Chem. Phys. Lett.* **421**, 469-472 (2006)

15. Yang, F. et al. Templated synthesis of single-walled carbon nanotubes with specific structure. *Acc. Chem. Res*. **49**, 606-615 (2016)
16. S. Zhang, et al. Arrays of horizontal carbon nanotubes of controlled chirality grown using designed catalysts. Nature 543, 234-238 (2017).
17. Sanchez-Valenca, J.R. et al. Controlled synthesis of single-chirality carbon nanotubes. *Nature* **512**, 61-64 (2014)
18. Rao, R., Eyink, K.G. & Maruyama, B. Single-walled carbon nanotube growth from liquid gallium and indium. *Carbon* **48**, 3971-3973 (2010)
19. Harutyunyan, A. R., Tokune, T. & Mora, E. Liquid as a required catalyst phase for carbon single-walled nanotube growth. *Appl. Phys. Lett*. **87**, 051919 (2005)
20. Harutyunyan, A.R., Tokune T., Mora E. Liquefaction of catalyst during carbon single-walled nanotube growth. Appl. Phys. Lett. 86, 153113 (2005)
21. Rao, R. et al. Graphene as an atomically thin interface for growth of vertically aligned carbon nanotubes. *Sci. Reports* **3**, 1891 (2013)
22. Popov, V.N., Henrad, L., Lambin, P. Resonant Raman intensity of the radial breathing mode of single-walled carbon nanotubes within a nonorthogonal tight-binding model. *Nano Lett.* **4**, 1795-1799 (2004)
23. Popov, V.N., Henrad, L., Lambin, P. Electron-phonon and electron-photon interactions and resonant Raman scattering from the radial-breathing mode of single-walled carbon nanotubes. *Phys. Rev. B* **72**, 035436 (2005)
24. Piao, Y. et al. Intensity ratio of resonant Raman modes for (n,m) enriched semiconducting carbon nanotubes. *ACS Nano* **10**, 5252-5259 (2016)
25. Harutyunyan, A.R., Pradhan, B.K., Kim, U.J., Chen, G., Eklund, P.C. CVD synthesis of single-wall carbon nanotubes under "soft" conditions. *Nano Lett.* **2**, 525-530 (2002)
26. Kalbac, M., et al. Defects in individual semiconducting single wall carbon nanotubes: Raman spectroscopic and in situ Raman spetroelectrochemical study. *Nano Lett*. **10,** 4619-4626 (2010)
27. Bachilo, S.M., et al. Narrow (n,m)-distribution of single-walled carbon nanotubes grown using a solid supported catalyst. *J. Am. Chem. Soc*. **125**, 11186-11187 (2003)
28. Miyauchi, Y., et al. Fluorescence spectroscopy of single-walled carbon nanotubes synthesized from alcohol. Chem. Phys. Lett. 387, 198-203 (2004)
29. Fouquet, M., et al. Highly chiral-selective growth of single-walled carbon nanotubes with a simple monometallic Co catalyst. *Phys. Rev. B* **85**, 235411-1- 235411-7 (2012)
30. Penev, E. S., Artyukhov, V. I. & Yakobson, B. I. Extensive Energy landscape sampling of nanotube end-caps reveals no chiral-angle bias for their nucleation. *ACS Nano* **8**, 1899-1906 (2014)
31. Artyukhov, V. I., Penev, E. S. & Yakobson, B. I. Why nanotubes grow chiral. *Nature Commun*. **5**, 4892 (2014)
32. Ding, F., Harutyunyan, A.R. & Yakobson, B.I. Dislocation theory of chirality-controlled nanotube growth. *Proc. Natl. Acad. Sci. USA* **106**, 2506-2509 (2009)

33. Rao, R., Liptak, D., Cherukuri, T., Yakobson, B.I. & Maruyama, B. In situ evidence for chirality-dependent growth rates of individual carbon nanotubes. *Nat. Mater.* **11**, 213-216 (2012)
34. Reich, S. & Robertson, J. Structure and formation of carbon nanotube caps. *Phys. Rev. B* **72**, 165423 (2005)
35. Rao, R., Sharma, R., Abild-Pedersen, F., Norskov, J.K. & Harutyunyan, A.R. Insights into carbon nanotube nucleation: Cap formation governed by catalyst interfacial step flow. *Sci. Rep.* **4**, 6510 (2014)
36. Brinkman, G., Fowler, P.W., Manolopoulos, D.E., Palser, A.H.R. A Census of nanotube caps. Chem. Phys. Lett. 315, 335-347 (1999).
37. Brinkmann, G., Fredrichs, O.D., Lisken, S., Peeters, A., Van Cleemput, N. CaGe – a Virtual environment for studying some special classes of plane graphs-an update. MATCH Commun. Comput. Chem. 63, 533-552 (2010).
38. J.H. ter Horst, D. Kashchiev, Determination of the nucleus size from the growth probability of clusters. J. Chem. Phys. 119, 2241-2246, (2003).
39. D. Kashchiev, Nucleation: Basic Theory with Applications, Butterworth-Heinemann, Oxford, 2000.
40. I. Markov, "Crystal Growth for beginners: Fundamentals of nucleation, Crystal growth and epitaxy" (World Scientific, Publ. Co. Pte. Ltd. 2nd Edition 2003).
41. Burton, W.K., Cabrera, N., Frank, F.C., The growth of crystals and the equilibrium structure of their surfaces. *Phil. Trans. Roy. Soc.* **243**, 299-358 (1951).

Support Information

The overall counts of the tubes grown on liquid Ga and solid Ru catalysts are shown in Table S1. The chirality abundances (in %) of detected SWNTs grown on liquid Ga droplets and solid Ru nanoparticles at various synthesis temperatures are presented in Tables S2-S7. Chirality distributions of carbon nanotubes grown on Ga catalyst at 925°C from three different runs under identical growth conditions are shown in Figure S.

Author information

Corresponding Author

*E-mail: aharutyunyan@honda-ri.com

The authors declare no competing financial interest.

Acknowledgements This work was supported by Honda Research Institute USA Inc. We thank R. Rao for synthesis of initial samples, E. Penev for helping with CaGe calculations, T. Maruyama for discussions of the results and S. Iijima and B. Yakobson for discussions of the results and the manuscript.

.

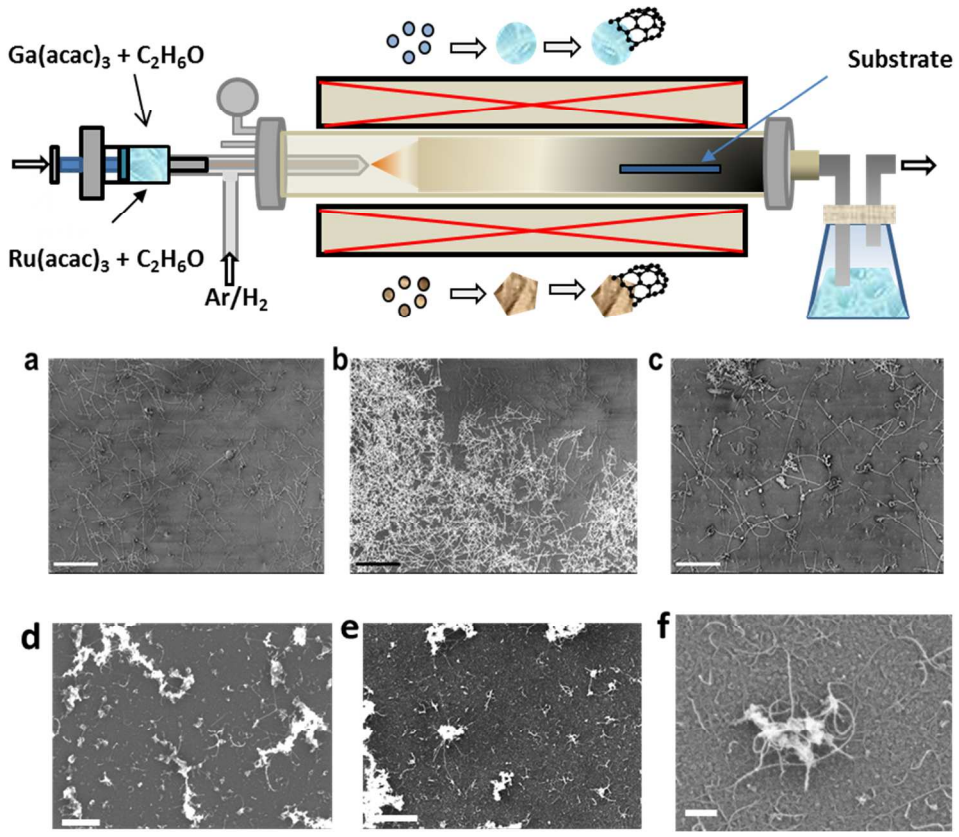

Figure 1: Schematic of the reactor for growth of single walled carbon nanotubes on floating catalysts. Representative SEM micrographs of SWNTs. a-c, Grown from $Ga(acac)_3$ at 900°C, 925°C, and 950°C, respectively. (d) Ru(acac) at 900°C, (e) Ru(acac) at 925°C, and (f) Ru(acac) at 950°C. Scale is 1 μm for all cases.

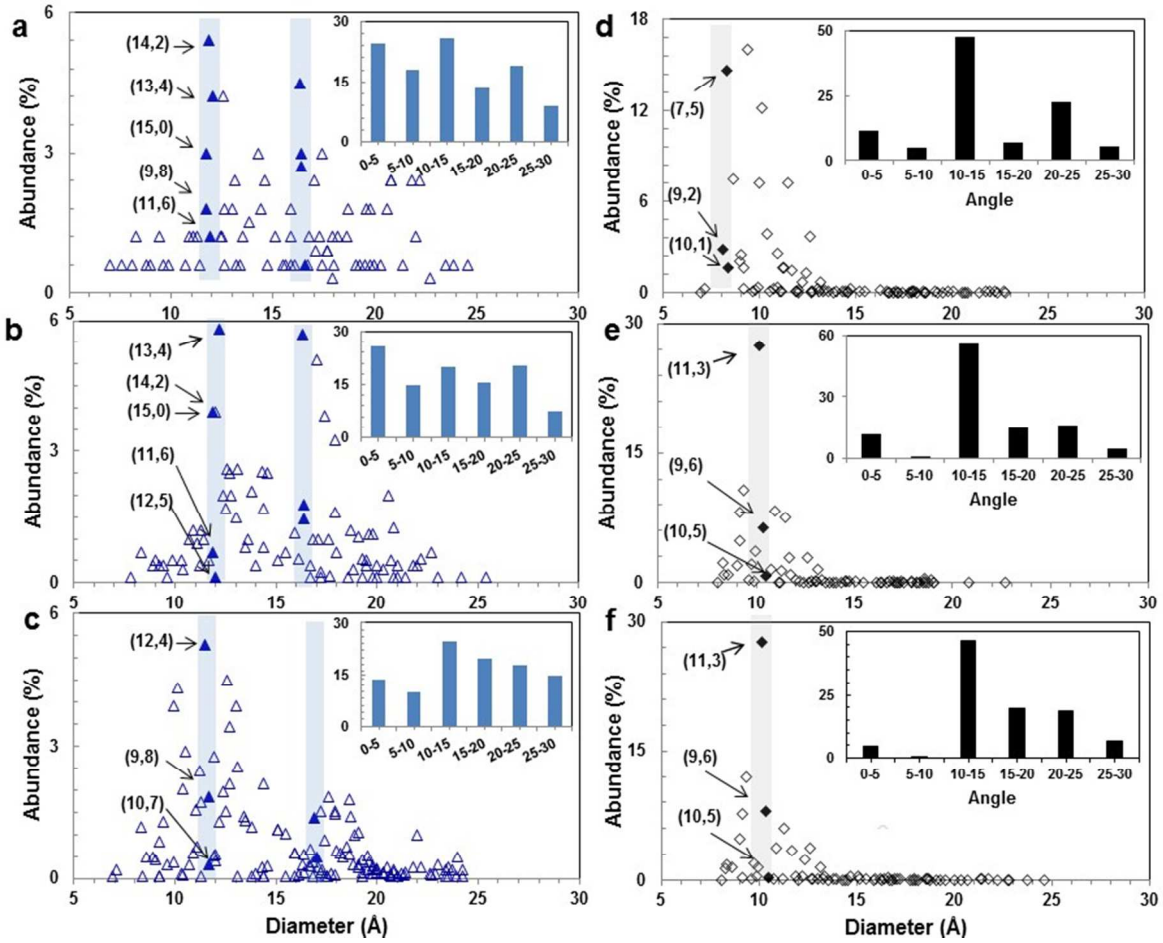

Figure 2: Abundances of SWNTs vs diameter based on corresponding Raman spectra. **a**, **b**, **c**, Grown on liquid Ga droplets. **e**, **f**, **g**, Grown on solid Ru catalysts at 900°C, 925°C and 950°C, respectively. Each experimental mark represents a nanotube with certain chirality (see Supporting Materials table S1-S6). Insets show the abundances of corresponding chiral-angles. Shadowed areas highlight the examples of abundance differences for the tubes with same nominal diameter (± 0.2Å) but different chiral angles.

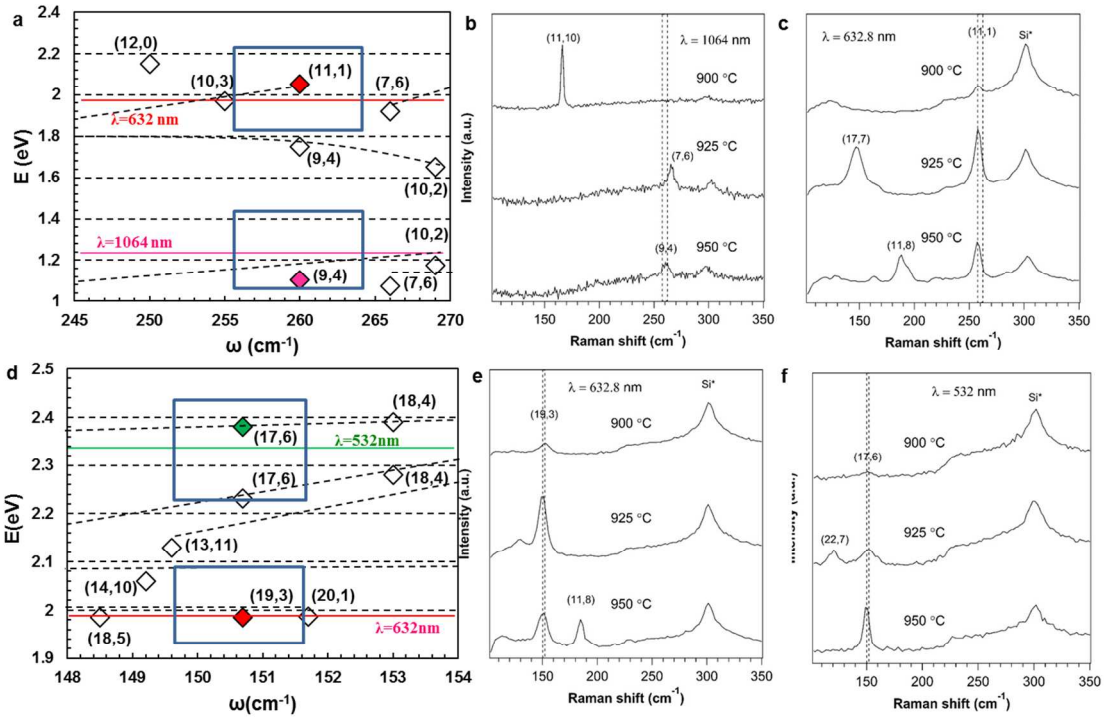

Figure 3: Theoretical Kataura Plot and representative Raman spectra for SWNTs grown on liquid Ga droplets. a, Kataura plot for the assignment of (9,4) and (11,1) chiralities. **b,c,** Corresponding representative Raman spectrum for the assignments in **(a)**. **d,** Kataura plot for the assignment of (17,6) and (19,3) chiralities. **e,f,** Corresponding representative Raman spectrum for the assignments in **(d)**. Solid lines in **(a, d)** indicate the excitation wavelengths and frames are the detection range, dashed lines in **(b, c, e, f)** are the detection ranges for the tubes with corresponding chiralities for various synthesis temperatures.

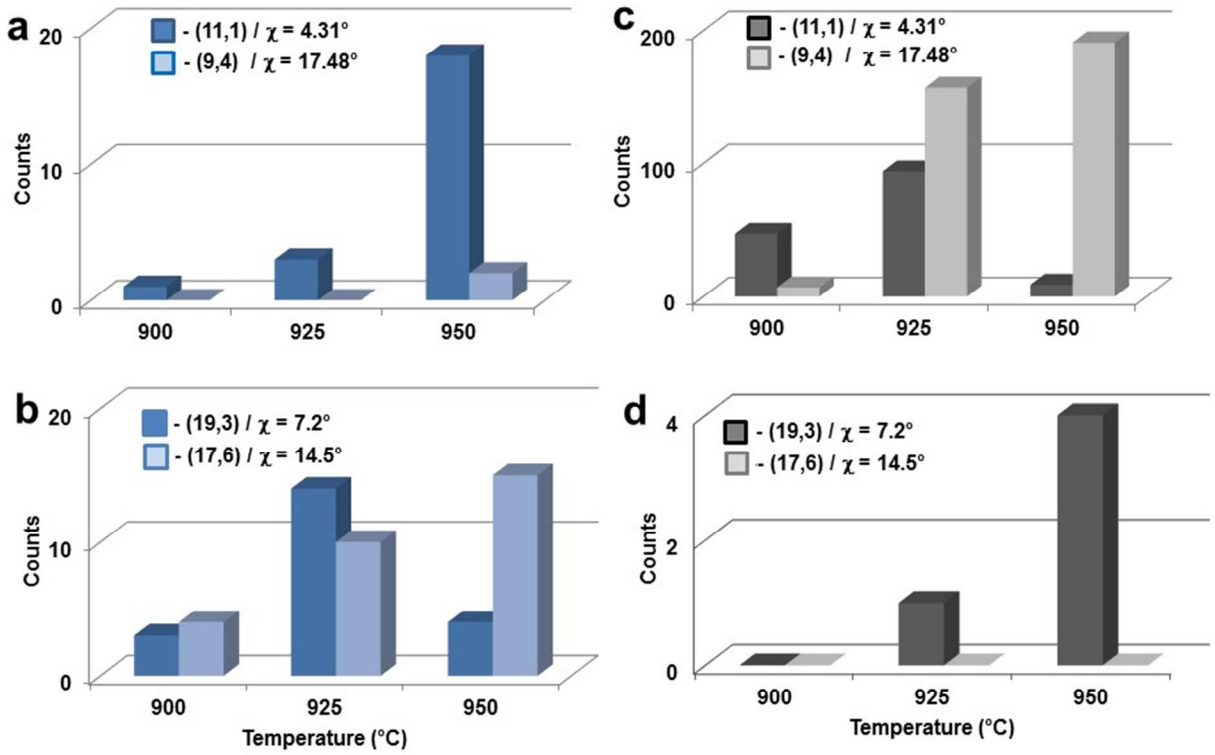

Figure 4: Abundances of SWNTs pairs (11,1)/(9,4) SWNTs with diameter d=9.156Å and (19,3)/17,6) with d=16.405Å vs. synthesis temperatures. **a, b**, Grown on liquid Ga droplets. **c, d,** Grown on solid Ru catalysts at 900°C, 925°C and 950°C, respectively. Estimated from corresponding Raman spectra.

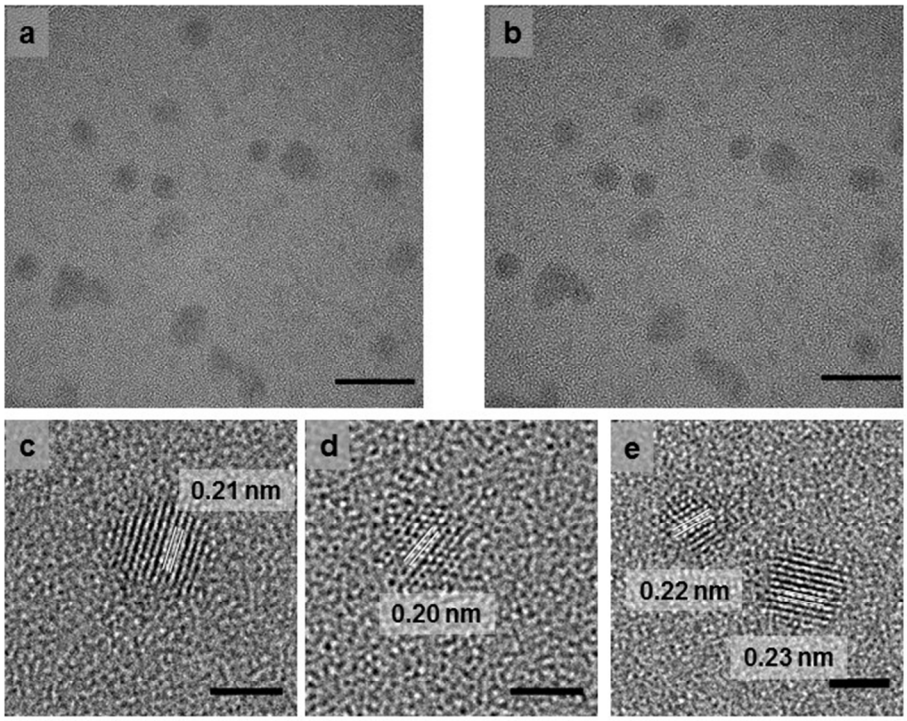

Figure 5: Characterization of catalyst particles. a, **b,** TEM images of Ru catalyst particles taken at 900 °C and 950 °C, respectively. **c-e** HRTEM images of catalyst particles taken at 950 °C. The interplanar spacings of Ru catalyst particles can be assigned as hcp (002) to c, hcp (101) to d, and hcp (002)-left and hcp (100)-right to e. Scale bars are 10 nm in **a,b** and 2 nm in **c-e**.

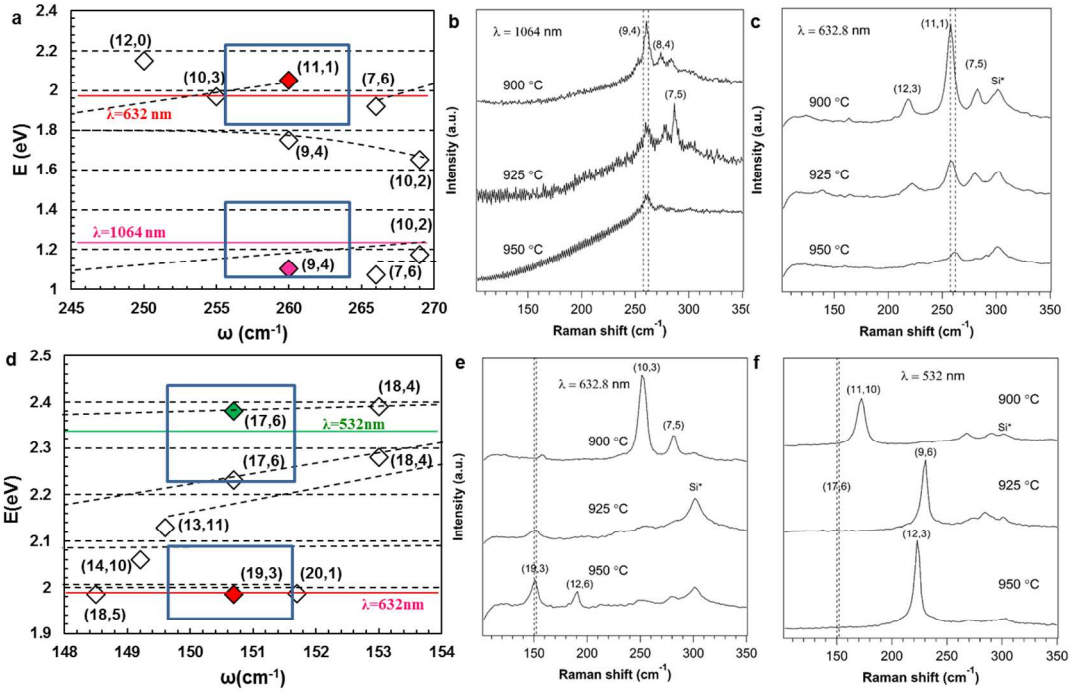

Figure 6: Theoretical Kataura Plot and representative Raman spectra for SWNTs grown on solid Ru nanoparticles. a, Kataura plot for the assignment of (9,4) and (11,1) chiralities. **b,c,** Corresponding representative Raman spectrum for the assignments in **(a)**. **d,** Kataura plot for the assignment of (17,6) and (19,3) chiralities. **e,f,** Corresponding representative Raman spectrum for the assignments in **(d)**. Solid lines in **(a, d)** indicate the excitation wavelengths and frames are the detection range, dashed lines in **(b, c, e, f)** are the detection ranges for the tubes with corresponding chiralities for various synthesis temperatures. (need to be replaced by actual Fig.)

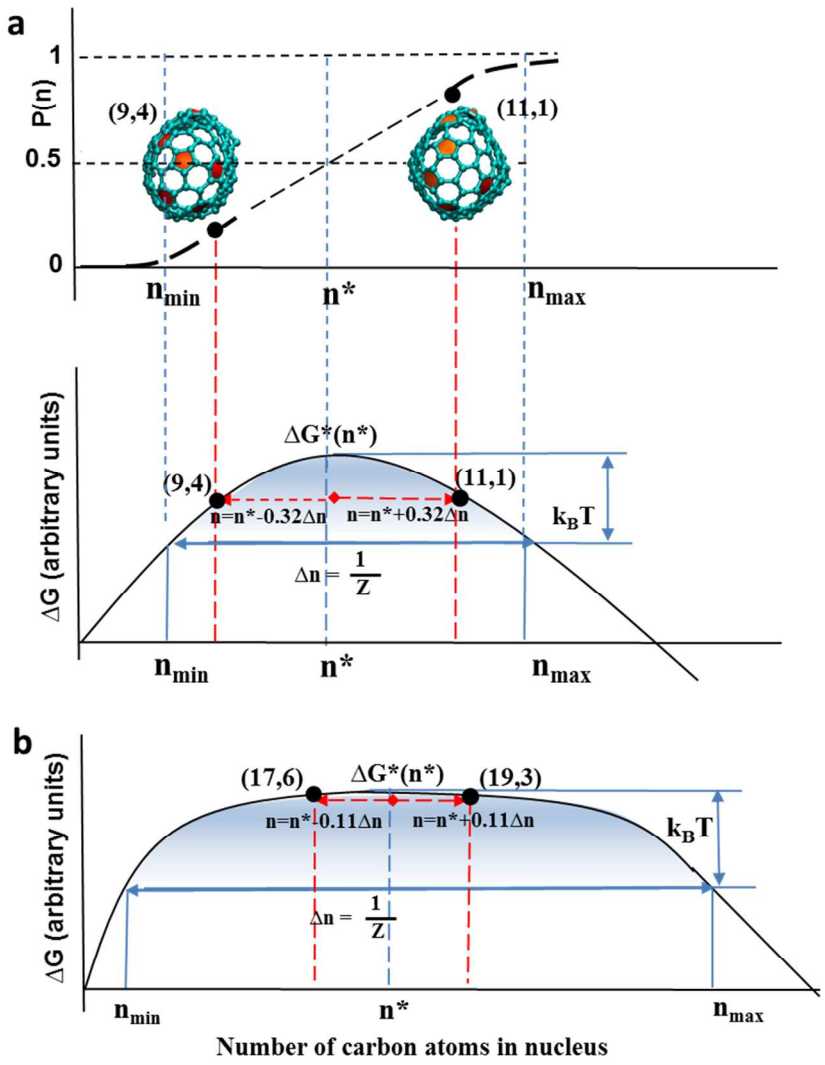

Figure 7. Gibbs free energy variation profiles for nuclei of tubes with same diameter but various chiralities and corresponding deviations from the energy of critical nuclei ΔG*(n*).

(a) For the (11,1) and (9,4) pair of tubes with the same diameter of d=9.156A grown at T=950^{o}C Top panel shows the corresponding values of these tubes on nucleation probability P(n) graph. **(b)** For the (19.3) and (17,6) pair of tubes with the same diameter of d= 16.405A grown at T=925^{o}C. Insets in the top panel of **(a)** show one of possible actual nanotube cap structures for corresponding chiralities.

Graphical